ferent tips, most likely due to changes in tip-induced electric field.
18. S. C. Lui, M. H. Kang, E. J. Mele, E. W. Plummer, D. M. Zehner, *Phys. Rev. B* **39**, 13149 (1989).
19. C. Kittel, *Introduction to Solid State Physics* (Wiley, New York, 1996).
20. The dI/dV signal is proportional to the DOS $\rho(E)$ in the quantum well with $\rho(E) = \Sigma c_n \, |\phi_n(k)|^2$. The corresponding energy levels $E_n(k)$ are eigenstates of the Schroedinger equation for wave functions $\phi_n(k)$. Wave functions in a 1D quantum well have the form $\phi_n(k) = {}^1\!/\!_2 \sin(kx)$ with $k = \pi n/L$. To determine the coefficients c_n, $\rho(E)$ is fitted to the observed dI/dV pattern.
21. S. LaShell, B. A. McDougall, E. Jensen, *Phys. Rev. Lett.* **77**, 3419 (1996).
22. K. N. Altmann *et al.*, *Phys. Rev. B* **64**, 035406 (2001).
23. E. Bertels, *Surf. Sci.* **331**, 1136 (1995).
24. A. Bogicevic *et al.*, *Phys. Rev. Lett.* **85**, 1910 (2000).
25. K. Swamy *et al.*, *Surf. Sci.* **482**, 402 (2001).
26. This material is based on work supported by the National Science Foundation under grant 0102887.
The award of a fellowship to N.N. by the Deutsche Forschungsgemeinschaft is gratefully acknowledged. We are greatly indebted to M. Persson for stimulating discussions and illuminating calculations. Additional insights have been provided by R. B. Muniz, D. L. Mills, and R. Wu.

19 June 2002; accepted 6 August 2002
Published online 22 August 2002;
10.1126/science.1075242
Include this information when citing this paper.

A Major Archean, Gold- and Crust-Forming Event in the Kaapvaal Craton, South Africa

Jason Kirk,[1*] Joaquin Ruiz,[1] John Chesley,[1] John Walshe,[2] Gavin England[3]

The 2.89- to 2.76-gigayear-old conglomerates of the Central Rand Group of South Africa host an immense concentration of gold. The gold and rounded pyrites from the conglomerates yield a rhenium-osmium isochron age of 3.03 ± 0.02 gigayears and an initial $^{187}Os/^{188}Os$ ratio of 0.1079 ± 0.0001. This age is older than that of the conglomerates. Thus, the gold is detrital and was not deposited by later hydrothermal fluids. This Middle Archean gold mineralization event corresponds to a period of rapid crustal growth in which much of the Kaapvaal craton was formed and is evidence for a significant noble metal flux from the mantle.

South Africa's Witwatersrand Supergroup (WSG) gold deposits have produced over 48,000 metric tons of gold and have accounted for about 40% of the world's total historic production (*1*). Attempts to date WSG gold mineralization remain equivocal, yielding a complex geochronology with ages that reflect multiple disturbances (*2–9*). Here, we determine the age of the gold mineralization to improve our understanding of the processes responsible for the changing styles and magnitudes of gold deposition.

The WSG, located in the Kaapvaal craton of South Africa (fig. S1), composes an ~7-km-thick sequence of detrital terriginous sediments (*2*, *10*) derived from the erosion of older granite-greenstone belts in fluvial deltaic settings (*11*). The WSG is divided into a lower West Rand Group and an upper Central Rand Group (CRG), with gold production largely confined to the quartz pebble conglomerates of the CRG (*1*). A maximum age for deposition of the CRG of 2.89 gigayears ago (Ga) has been obtained from the youngest detrital zircons found in the lower CRG (*12*), and a minimum age of 2.76 Ga was determined based on the oldest authigenic xenotime Pb ages in the CRG (*9*).

Geochronology of the WSG provenance includes U-Pb ages on detrital zircons and monazites, which yield an age range from 3.3 to 2.8 Ga (fig. S1). U-Pb and Pb-Pb isotopic ages from rounded uraninite (*3*) and pyrite grains (*4*), as well as Os isotopic model ages from osmiridium grains (*5*) and gold grains (*6*), are all between about 3.5 and 2.9 Ga, and thus these phases have been interpreted as being of detrital origin (fig. S1). U-Pb and Pb-Pb ages on pyrites, uraninites, hydrothermal zircon, rutile, and xenotime, as well as K-Ar ages on clays and micas, are between about 2.7 and 2.0 Ga (*1*, *2*, *7*, *9*). These younger ages have been used to define a series of at least five tectonothermal events that may have introduced and/or mobilized gold (fig. S1).

The superimposed metamorphism on the conglomerate hosts of the WSG has led to contentious debate on the age and origin of gold, centered around placer and epigenetic models. In placer models, gold and associated rounded pyrite are detritus from unidentified

[1]Department of Geosciences, University of Arizona, Tucson, AZ 85721, USA. [2]Commonwealth Scientific and Industrial Research Organisation, Division of Exploration and Mining, 39 Fairway, Nedlands 6009, Western Australia. [3]Geology and Geophysics Department, University of Edinburgh, Edinburgh EH9 3JW UK.

*To whom correspondence should be addressed. E-mail: jkirk@geo.arizona.edu

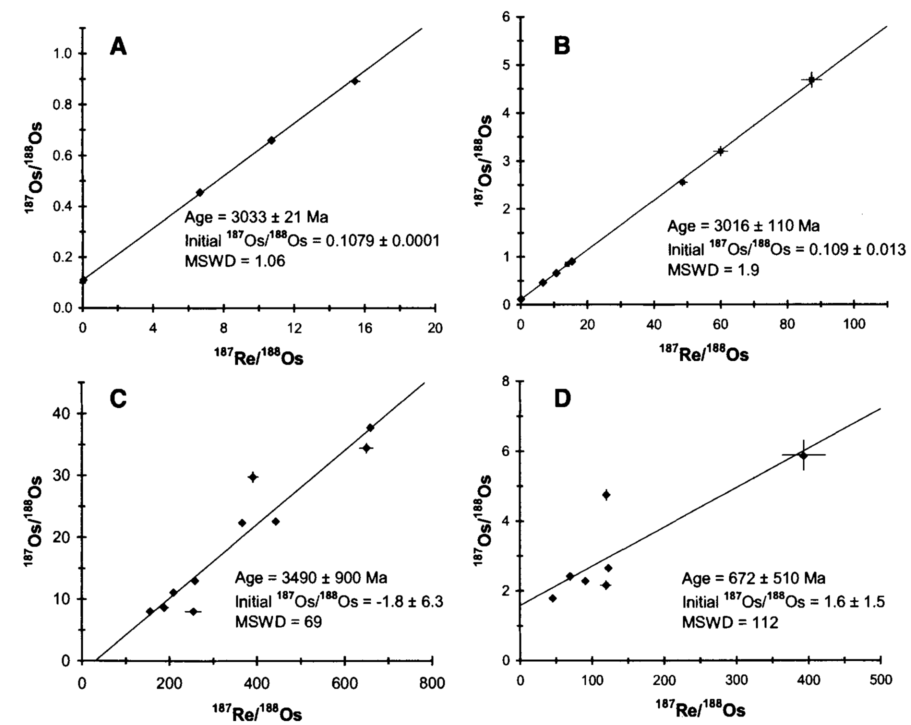

Fig. 1. Re-Os isochron diagrams for WSG samples. In all isochrons, errors are represented by crosses or are smaller than the symbols used. Errors were determined by using the greater of either the 2σ counting error ($2SD\sqrt{n}$) or by varying the Os blank between measured values of 1 to 2 pg. All isochrons were calculated using Isoplot (*25*). (**A**) VR gold samples. (**B**) VR gold and rounded VR pyrites. Filled squares represent pyrite samples; filled diamonds represent gold samples. (**C**) SR rounded pyrite samples. (**D**) VCR euhedral pyrites.

source rock(s) older than the age of host conglomerate deposition (*13*, *14*). Epigenetic models propose that gold was introduced into the host conglomerates after deposition by hydrothermal/metamorphic fluids derived from the upper continental crust (*15–17*). Between these two end-member models, modified placer models incorporate detrital gold and modification by later hydrothermal fluids (*1*, *2*). The clearest discriminator between these models is the age of the gold mineralization.

Re and Os are concentrated in sulfides and metals (*6*, *18*), thus allowing for the direct dating of gold and pyrite using the decay of ^{187}Re to ^{187}Os. The initial Os isotopic composition of the gold also constrains the potential source region(s). Crustal rocks will develop elevated $^{187}Os/^{188}Os$ values rapidly because of high Re/Os ratios relative to the mantle (*18*).

Gold with morphologies interpreted to be of detrital and authigenic origin has been recognized in the WSG (*19*). To constrain the origin of the gold, we analyzed Vaal Reef (VR) gold samples associated with carbonaceous material and mostly authigenic in appearance. We also analyzed pyrite grains interpreted to be of detrital, diagenetic, and authigenic origin (*1*, *2*) from the VR, Steyn Reef (SR), and Ventersdorp Contact Reef (VCR) (*20*) (fig. S1, Table 1).

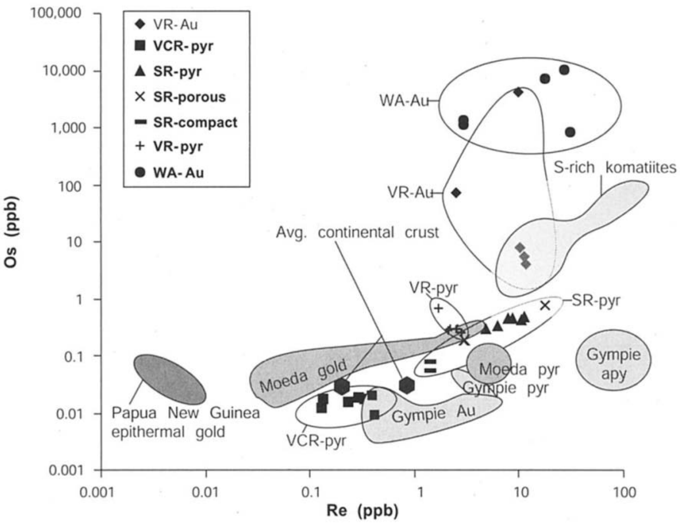

Fig. 2. Re concentration versus Os concentration data from gold and pyrite data from this study, (*6*), and (*21*). Circles represent analyses of gold from the Western Areas Gold Plant (~70:30 mixture of Upper Elsberg and Ventersdorp Contact Reefs from the Carletonville Goldfield); diamonds represent VR gold; plus symbols represent VR rounded pyrites; squares represent VCR cubic pyrites; triangles represent Steyn Reef rounded pyrite samples; and X's and dashes represent SR porous rounded pyrites and compact rounded pyrites, respectively. Sulfur-rich komatiite field is from (*26*). Filled hexagons represent two estimates of average continental crust (*27*, *28*).

Table 1. Re and Os concentrations and isotopic compositions. cpt-rd: compact round pyrite; por-rd: porous round pyrite; rd-pyr: rounded pyrite of both porous and compact morphologies.

Sample name	Re (ppb)	Os (ppb)	$^{187}Re/^{188}Os$	$^{187}Os/^{188}Os$
		Vaal Reef		
VR-Au-1*	9.86	4162	0.0116 ± 0.0168†	0.10848 ± 0.00004†
VR-Au-2*	2.47	73.1	0.151	
VR-Au-5	10.3	8.02	6.66 ± 0.06	0.45429 ± 0.00243
VR-Au-6	11.2	5.42	10.72 ± 0.10	0.66020 ± 0.00431
VR-Au-7	11.4	4.05	15.46 ± 0.33	0.89166 ± 0.01531
VR-rd-pyrite-1*	1.72	0.68	14.00 ± 0.28	0.84 ± 0.01
VR-rd-pyrite-2*	2.20	0.30	48.54 ± 1.60	2.55 ± 0.08
VR-rd-pyrite-3*	2.60	0.30	60.08 ± 2.29	3.20 ± 0.11
VR-rd-pyrite-4*	2.80	0.26	87.31 ± 3.25	4.68 ± 0.17
		Ventersdorp Contact Reef (Footwall)		
VCR-FW-pyr-1	0.33	0.018	119.04 ± 7.98	2.16 ± 0.13
VCR-FW-pyr-2	0.13	0.012	69.75 ± 3.63	2.40 ± 0.12
VCR-FW-pyr-3	0.23	0.016	91.73 ± 3.21	2.28 ± 0.08
VCR-FW-pyr-4	0.41	0.009	393.47 ± 30.3	5.88 ± 0.44
VCR-FW-pyr-5	0.39	0.020	124.16 ± 2.98	2.64 ± 0.06
VCR-FW-pyr-6	0.29	0.019	120.11 ± 4.56	4.74 ± 0.18
VCR-FW-pyr-7	0.13	0.018	45.78 ± 1.24	1.77 ± 0.05
		Steyn Reef		
SR-rd-pyr-1	10.5	0.43	649.95 ± 16.3	34.43 ± 0.86
SR-rd-pyr-2	8.79	0.44	258.84 ± 2.85	13.01 ± 0.14
SR-rd-pyr-3	7.79	0.44	209.54 ± 2.30	11.19 ± 0.12
SR-rd-pyr-4	6.25	0.32	367.31 ± 8.63	22.30 ± 0.52
SR-rd-pyr-5	4.87	0.29	391.18 ± 12.5	29.76 ± 0.95
SR-rd-pyr-6	11.2	0.48	442.34 ± 3.54	22.63 ± 0.18
SR-por-rd-1	17.9	0.77	659.26 ± 4.15	37.64 ± 0.24
SR-por-rd-2	2.91	0.18	157.23 ± 3.14	7.98 ± 0.16
SR-cpt-rd-1	1.40	0.06	254.72 ± 19.1	8.01 ± 0.60
SR-cpt-rd-2	1.41	0.08	187.42 ± 11.1	8.67 ± 0.51

*Data are from (*6*). †Errors were calculated using the greater of either 2σ instrumental error ($2SD\sqrt{n}$) or by varying the Os blank between measured values of 1 to 2 pg ($^{187}Os/^{188}Os$ = 0.181). Highest source of error in the $^{187}Re/^{188}Os$ ratio for VR-Au-1 was from varying the Re blank between measured values of 10 to 15 pg.

Data from VR gold define a linear array on a Re-Os isochron diagram (Fig. 1A) and yield an age of 3.01 ± 0.11 Ga [mean square weighted deviation (MSWD) = 1.9] and have an initial $^{187}Os/^{188}Os$ value of 0.109 ± 0.013. Rounded VR pyrites yield an isochron age of 2.99 ± 0.11 Ga (MSWD = 0.77) and an initial $^{187}Os/^{188}Os$ value of 0.124 ± 0.036 (*6*). Combining both VR gold and rounded pyrite from the same hand sample gives a more precise age of 3.03 ± 0.02 (MSWD = 1.06) and an initial $^{187}Os/^{188}Os$ value of 0.1079 ± 0.0001 (Fig. 1B).

Rounded SR pyrites are consistent with the ~3.0-Ga VR gold and pyrite isochron, yielding an age of 3.49 ± 0.90 Ga (MSWD = 69) (Fig. 1C). The Os isotopic composition of the compact rounded and porous rounded SR pyrite separates is within the range of SR rounded pyrites not separated by morphology, but the porous pyrites have higher Os concentrations than the compact variety. Photomicrograph images of porous pyrites show authigenic pyrite and gold within the porous round pyrite grains (*20*). These gold inclusions may explain both the higher Os concentrations of the porous SR pyrites and the relatively larger scatter in the SR pyrite data.

The data obtained in this study indicate that VR gold is older than the host CRG conglomerates (2.89 to 2.76 Ga). The rounded VR and SR pyrite samples also predate their host. These ages are strong evidence that the gold and rounded pyrite mineralization predate deposition of the conglomerate host and are thus originally detrital.

Authigenic pyrites from the VCR were examined to test for possible effects of hydrothermal alteration on gold and rounded pyrite. The voluminous, relatively impermeable flood basalts of the Ventersdorp Supergroup overlying the VCR make it arguably the most intensely hydrothermally altered conglomerate host of the WSG (*1*, *7*). The cubic VCR pyrites analyzed are epigenetic in origin, and therefore the Os compositions of the VCR pyrites reflect the Os composition of the epigenetic fluids responsible for their precipitation.

Re-Os data for authigenic VCR pyrites (*20*) are relatively scattered on an isochron diagram. The data plot between 2.4 and 0.3 Ga reference isochrons and yield an age of 672 ± 510 million years (MSWD = 112) with an initial $^{187}Os/^{188}Os$ value of 1.6 ± 1.5 (Fig. 1D). The VCR pyrites have low Os concentrations (9 to 20 parts per trillion); therefore, their Os isotopic compositions are more prone to being altered through interactions with later Os-bearing fluids than VR gold and pyrite with higher Os concentrations. The scattered distribution of the VCR pyrite Re-Os data likely has no age relevance, but rather reflects postdepositional disturbance or averaging of different authigenic generations of VCR pyrite.

VR gold and pyrite have much larger Os concentrations than the VCR pyrite (Table 1), suggesting a deposition mechanism different from the epigenetic precipitation of the VCR pyrite. The higher Os concentrations of the VR gold and pyrite would also imply that their geochronologic information is more unlikely to have been disturbed by later precipitation or mobilization of Os by hydrothermal fluids.

A mantle or mantle-derived mafic/ultramafic rock source for the WSG gold and rounded pyrite is indicated by initial $^{187}Os/^{188}Os$ values of 0.109 (VR-Au isochron) and 0.108 (VR-Au and Pyr isochron), corresponding to the estimated Os isotopic composition of the mantle at about 3.0 Ga (*6*). Supporting evidence for a mantle origin of WSG gold is provided by the higher Os concentration of the WSG gold relative to the VCR pyrite, the gold and pyrite from other hydrothermal gold deposits, and the younger (~2.2 Ga) Moeda Formation paleoplacer deposit (Fig. 2) (*21*, *22*). Minerals from these younger deposits have low Os concentrations and high Re/Os ratios similar to those of evolved crustal rocks. The WSG gold, and to a lesser extent rounded pyrites, have high Os concentrations and low Re/Os ratios more similar to those of mantle rocks and primary S-rich komatiites (Fig. 2).

The age of the VR gold and pyrite may reflect the age of the mineralization event in the source rock(s) they were derived from, whereas the initial $^{187}Os/^{188}Os$ value constrains the source area of that rock. When plotted together, the VR gold and pyrites yield a precise age of 3.03 ± 0.02 Ga with a homogeneous, unradiogenic (mantle-like) initial value and may indicate that both gold and pyrite mineralization are cogenetic. This age is similar to the 3.08-Ga peak in WSG detrital zircon ages (*2*). Zircons of this age reflect an increasing evolved granitic crustal input, as well as an increase in basaltic/greenstone components delivered to the WSG sediments. These components are possibly derived from erosion of 3.08-Ga basalts of the Dominion Group and the 3.07- to 2.97-Ga Murchison greenstone belt (*2*, *23*). Although the Dominion Group is not a likely source of large amounts of gold, contemporaneous subaqueous expressions of mafic magmatism in the form of gold-rich sulfide-facies exhalites may have been a potential source (*24*). The Murchison greenstone belt and possible equivalents along the Thabazimbi-Murchison lineament are candidates for the source of gold to the WSG (*23*). The initial $^{187}Os/^{188}Os$ value of WSG gold (0.109) is consistent with gold emplacement into the crust by mantle-derived basaltic/greenstone magmatism at ~3.0 Ga.

References and Notes

1. H. E. Frimmel, W. E. L. Minter, *Soc. Econ. Geol. Spec. Publ.* **9**, 17 (2002).
2. L. J. Robb, F. M. Meyer, *Ore Geol. Rev.* **10**, 67 (1995).
3. C. C. Rundle, N. J. Snelling, *Philos. Trans. R. Soc. London Ser. A* **286**, 567 (1977).
4. R. Saager, *U.S. Geol. Surv. Prof. Pap.* **1161-L**, 1 (1981).
5. S. R. Hart, E. D. Kinloch, *Econ. Geol.* **84**, 1651 (1989).
6. J. Kirk, J. Ruiz, J. Chesley, S. Titley, J. Walshe, *Geochim. Cosmochim. Acta* **65**, 2149 (2001).
7. R. E. Zartman, H. E. Frimmel, *Mineral. Petrol.* **66**, 171 (1999).
8. H. E. Frimmel, *J. Geol.* **105**, 601 (1997).
9. G. L. England *et al.*, *Terra Nova* **13**, 1 (2001).
10. M. P. Coward, R. M. Spencer, C. E. Spencer, in *Early Precambrian Processes*, M. P. Coward, A. C. Reis, Eds. (Geological Society of London, Spec. Publ. 95, 1995), p. 243.
11. W. E. L. Minter, *Min. Eng.* **42**, 195 (1990).
12. M. Poujol, L. J. Robb, J. P. Respaut, *Precambrian Res.* **95**, 167 (1999).
13. E. T. Mellor, *Trans. Inst. Min. Metall.* **25**, 226 (1916).
14. D. K. Hallbauer, T. Utter, *Miner. Deposita* **12**, 296 (1977).
15. L. C. Graton, *Econ. Geol.* **25** (suppl. 3), 1 (1930).
16. G. N. Phillips, D. M. Law, *Ore Geol. Rev.* **9**, 1 (1994).
17. A. C. Barnicoat *et al.*, *Nature* **386**, 820 (1997).
18. S. B. Shirey, R. J. Walker, *Annu. Rev. Earth Planet. Sci.* **26**, 423 (1998).
19. W. E. L. Minter, *Econ. Geol.* **94**, 665 (1999).
20. Materials and methods are available as supporting material on *Science* Online.
21. J. Kirk, unpublished data.
22. W. E. L. Minter, F. E. Renger, A. Siegers, *Econ. Geol.* **85**, 943 (1990).
23. M. Poujol, L. J. Robb, J. P. Respaut, C. R. Anhaeusser, *Econ. Geol.* **91**, 1455 (1996).
24. R. W. Hutchinson, R. P. Viljoen, *S. Afr. J. Geol.* **91**, 157 (1988).
25. K. R. Ludwig, *U.S. Geol. Surv. Open File Rep.* 91-445 (1991).
26. D. D. Lambert, J. G. Foster, L. R. Frick, *Econ. Geol.* **93**, 121 (1998).
27. B. K. Esser, K. K. Turekian, *Geochim. Cosmochim. Acta* **57**, 3093 (1993).
28. B. Peucker-Ehrenbrink, B. Jahn, G^3 **2**, paper no. GC000172 (2001).

29. We thank M. Baker for managing the isotopic laboratory and N. Fox (AngloGold) for help with providing Vaal Reef samples. We appreciate thoughtful reviews by F. Barra, R. Mathur, Z. Naiman, and three anonymous reviewers that improved this manuscript. Analytical work was funded by the National Science Foundation (grants EAR 9708361 and EAR 9628150). Re-Os analyses were performed at the Keck laboratory, University of Arizona.

Supporting Online Material

www.sciencemag.org/cgi/content/full/297/5588/1856/DC1
Material and Methods
Fig. S1

19 June 2002; accepted 31 July 2002

Deformation on Nearby Faults Induced by the 1999 Hector Mine Earthquake

Yuri Fialko,[1*] David Sandwell,[1] Duncan Agnew,[1] Mark Simons,[2] Peter Shearer,[1] Bernard Minster[1]

Interferometric Synthetic Aperture Radar observations of surface deformation due to the 1999 Hector Mine earthquake reveal motion on several nearby faults of the eastern California shear zone. We document both vertical and horizontal displacements of several millimeters to several centimeters across kilometer-wide zones centered on pre-existing faults. Portions of some faults experienced retrograde (that is, opposite to their long-term geologic slip) motion during or shortly after the earthquake. The observed deformation likely represents elastic response of compliant fault zones to the permanent co-seismic stress changes. The induced fault displacements imply decreases in the effective shear modulus within the kilometer-wide fault zones, indicating that the latter are mechanically distinct from the ambient crustal rocks.

Stress and strain transfer within seismogenic fault systems is a well-documented yet poorly understood phenomenon. It is known that earthquakes can activate nearby (or, sometimes, distant) faults, causing variations in local seismicity rates or triggering aseismic fault slip (*1*–*3*). Detailed studies using Interferometric Synthetic Aperture Radar (InSAR) data from several large strike-slip earthquakes, including the 1992 M_w7.3 Landers earthquake (where M_w is the moment magnitude) (*4*), the 1999 M_w7.6 Izmit earthquake (*5*), and the 1999 M_w7.1 Hector Mine earthquake (*6*, *7*), revealed ubiquitous displacements on pre-existing faults in the vicinity of the mainshock rupture. In some instances, the sense of fault motion has been

[1]Institute of Geophysics and Planetary Physics, Scripps Institution of Oceanography, University of California San Diego, La Jolla, CA 92093, USA. [2]Seismological Laboratory, Division of Geological and Planetary Sciences, California Institute of Technology, Pasadena, CA 91125 USA.

*To whom correspondence should be addressed. E-mail: fialko@radar.ucsd.edu.